Energy Distribution of Protons from a Target Bombarded by 190-Mev Deuterons

WARREN W. CHUPP, EUGENE GARDNER, AND T. B. TAYLOR
Radiation Laboratory, Department of Physics, University of California, Berkeley, California

(Received December 22, 1947)

Previous experimental work by Helmholz, McMillan, and Sewell has shown that a narrow beam of high energy neutrons is produced when a beam of 190-Mev deuterons strikes a thin target. The mechanism for the production of the neutrons has been discussed by Serber, who describes a process in which the proton in the deuteron strikes the edge of a nucleus in the target and is stripped off, while the neutron misses and continues on its way. It is to be expected that an equal number of high energy protons are produced by stripping processes in which it is the neutron that hits the nucleus. These high energy protons have been detected by (1) carbon activation, and (2) photographic plates. Both methods give energy distributions in agreement with the energy distribution predicted for protons produced by the stripping process.

1. INTRODUCTION

THE neutrons coming from the target of the 184-inch Berkeley cyclotron[1] have been studied experimentally by Helmholz, McMillan, and Sewell.[2] The mechanism for the production of the neutrons from the deuteron beam has been discussed by Serber,[3] who describes a process in which the proton in the deuteron strikes the edge of the nucleus and is stripped off, while the neutron misses and continues on its way. It is pointed out by Serber that an equal number of high energy protons are produced at the target by stripping processes in which it is the neutron that hits the nucleus. The object of the present investigation was to detect these protons and to measure their energy distribution. Professor L. W. Alvarez called attention to the fact that the magnetic field of the cyclotron provides a convenient means of separating protons of different energies, since the radii of curvature of the proton trajectories will be proportional to the momenta of the protons.

Two different methods were used for detecting the protons: (1) carbon activation, and (2) photographic plates, experimentation with the two methods being carried on concurrently. It was found that the data could be obtained faster and more reliably by the carbon activation method, and the results from this method are considered to be much more accurate than those from the photographic plate method. The results from the photographic plate method will be included, however, in order to corroborate the findings of the carbon activation method and to give information which may be of interest in connection with future applications of the photographic plate method.

2. CARBON ACTIVATION METHOD

It was pointed out by Professor E. M. McMillan that the reaction $C^{12}(p,pn)C^{11}$ provides a convenient method of studying protons from the target, since the cross section for this reaction is essentially constant in the range of energies from 60 Mev to at least 140 Mev.[4] The general arrangement of the carbon detectors in the cyclotron is shown in Fig. 1. For each of the different radial positions shown in the figure there were several carbon plates of dimensions 3 inches by 4 inches by $\frac{3}{16}$ inch. The $\frac{3}{16}$-inch dimension was in the direction of motion of the protons, and the plates were placed one behind another so that the proton beam passed through several plates in succession. Enough plates were provided so that the plates extended approximately 2 inches beyond the calculated range of the protons. The carbon plates were surrounded by lead plates of 1-inch thickness, and the protons were admitted through an aperture in the lead shielding which was $1\frac{1}{2}$ inches high by 2 inches

[1] Brobeck, Lawrence, MacKenzie, McMillan, Serber, Sewell, Simpson, and Thornton, Phys. Rev. **71**, 449 (1947).
[2] A. C. Helmholz, Edwin M. McMillan, and Duane C. Sewell, Phys. Rev. **72**, 1003 (1947).
[3] R. Serber, Phys. Rev. **72**, 1008 (1947).
[4] W. W. Chupp and E. M. McMillan, Phys. Rev. **72**, 873 (1947).

wide. The shielding system was extended 10 inches in front of the carbon blocks, and at this position there was another aperture which admitted all trajectories of horizontal angle up to $\pm 10°$ which could strike the $1\frac{1}{2}$-inch by 2-inch opening at the carbon blocks. The horizontal angle of a trajectory refers to the horizontal angle at which the trajectory leaves the target, the direction of the deuteron beam being taken as zero. As shown in Fig. 1, the protons leaving the target describe an arc of 150° before striking the detectors. At the 150° position, the trajectories at various horizontal angles do not come together as nicely as they do at 180° position. However, the 150° position is sufficiently close to the 180° position so that the spread in energies at the detectors is only about ± 9 percent for all energies under consideration. The magnetic field of the 184-inch cyclotron is about 5 percent smaller at a radius of 80 inches than at the center. In order to find the effect on the proton trajectories of this change in magnetic field, several trajectories were plotted graphically. The effect of the variation in magnetic field was found to be much smaller than the ± 9 percent energy spread mentioned above.

The activity in the carbon detectors is a resultant of the effects of protons, deuterons, and neutrons. The deuterons come from the vicinity of the target, where they are scattered from the edge of the dee. They can pass through varying thicknesses of copper in the dee depending on their angle of incidence, and hence can appear at the detectors at any momentum position. At any given detector position the deuterons have the same momentum as the protons and hence have half the energy. The method of separating the effects of the protons, deuterons, and neutrons was to measure the activities of three plates at each detector position. One plate, at or near the position where the beam first strikes the stack of plates, measured the total effect of the protons plus the deuterons plus the neutrons. Another plate, placed beyond the end of the deuteron range but not so far along that the protons had energies less than 60 Mev, measured the effect of the protons plus the neutrons. Still another plate, placed well beyond the range of the protons, measured the effect of the neutrons only.

With the detectors in place in the cyclotron, a copper target of thickness $\frac{1}{16}$ inch was bombarded with 190-Mev deuterons for about 20 minutes. The carbon plates were then removed from the vacuum chamber, and activities were measured. The activities were all corrected to some arbitrarily chosen time after bombardment. Each plate was counted at least five times to check the decay curve. Two runs were made, the second run to obtain points approximately midway between those of the first. The first run showed that there were many deuterons present; large numbers of deuterons at the detectors are objectionable because of stripping of the deuterons in the detectors, with a consequent increase in the neutron background. The deuterons were largely removed from the region of the detectors during the second run by inserting a C-shaped defining slot in the dee 90° "ahead" of the target. The open end of the slot was directed toward the ion source, and the horizontal arms defined the deuteron beam to a 3 inch vertical height. This gave a 1-inch clearance from

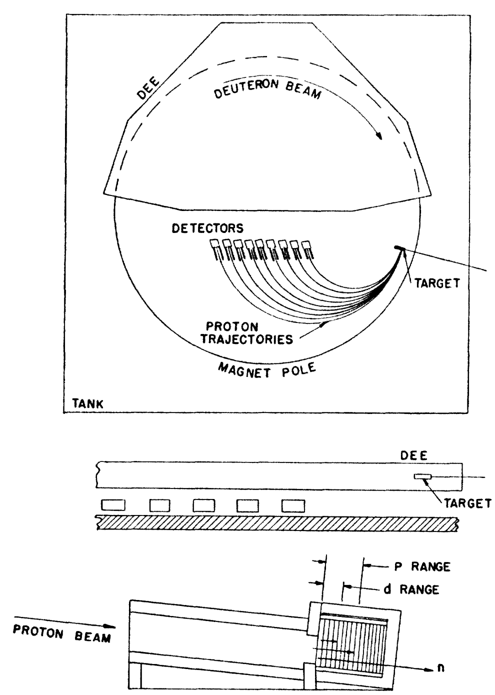

FIG. 1. Arrangement of apparatus used with carbon activation method. Top: plan view of cyclotron showing carbon detectors in position. Middle: portion of front view of cyclotron showing carbon detectors in position just below the dee. Bottom: detail showing carbon detectors surrounded by lead shielding.

TABLE I. Data from carbon activation method.

Position	ρ radius inches	E Mev	Activity due to $p+n$	Activity due to n	Total activity d, p, and n	Activity due to p	Proton activity multiplied by radius and normalized	First run only data multiplied by 0.94 to correlate with second run
2	30	57.2	2300	250	2300	2050	0.212	0.200
$2\frac{1}{2}$	31.75	64.1	1220	74	1290	1146	0.282	
3	33.5	70.5	5300	158	5300	5142	0.595	0.560
$3\frac{1}{2}$	35.25	78.7	2800	53	3000	2747	0.751	
4	37	87.0	7600	122	7800	7478	0.955	0.90
$4\frac{1}{2}$	38.75	95.4	3380	49	3520	3331	1.00	
5	40.5	104	5000	107	5200	4893	0.683	0.643
$5\frac{1}{2}$	42.25	113	1400	46	1700	1354	0.443	
6	44	123	1625	115	2700	1510	0.230	0.217
$6\frac{1}{2}$	45.75	133	490	46	870	444	0.157	
7	47.5	151	710	73	5200	637	0.105	0.099
8	51.0	165	305	95	7300	210	0.037	0.035
9	54.5	188	273	150	15500	123	0.023	0.022

the top and bottom of the dee. The removal of these deuterons did not change the observed proton distribution noticeably.

The results of the activity measurements are given in Table I. The activities in this table do not give directly the numbers of protons in the various momentum intervals because the detectors, being of fixed height, do not subtend the same vertical angles. It can be shown that the number of protons striking an area A at the detector is proportional to A/L, where L is the length of the trajectory from target to detector. If R_p is the radius of the proton path, then for the 150° position

$$L = 5\pi R_p/6.$$

Thus, in order to find the numbers of protons in the various momentum intervals, it is necessary to multiply the observed activities by the proton trajectory radii. The products of the observed

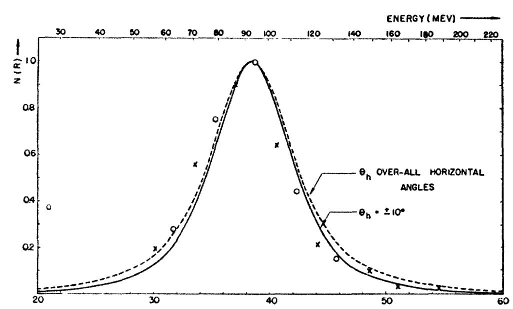

FIG. 2. Distribution measured with carbon detectors. Ordinate gives numbers of protons in various momentum intervals. Crosses, run 1; circles, run 2. θ_h = horizontal angle at which trajectory leaves the target. The curves are calculated distributions on the basis of a transparent nuclear model.

activities and the radii have been plotted in Fig. 2. The data from the two runs have been normalized to fit on a smooth curve. Corrections for target loss have been applied to the calculated distribution curves, as will be explained in Section 4.

In order to be able to compare the experimental points of Fig. 2 with the calculated curve, we measured the proton energy at one detector position by means of the proton range. At the position used for the measurement, the proton trajectory radius was $37\frac{1}{4}$ inches, and the energy was found to be 88 Mev. From the radius and the energy it is possible to calculate the effective magnetic field. The value found in this way was 14.62 kilogauss, which corresponds very closely to the average of the magnetic field at the center of the cyclotron and the magnetic field at 80 inches from the center.

3. PHOTOGRAPHIC PLATE METHOD

When photographic plates[5,6] were used as detectors, the numbers of protons in the various momentum intervals were found by counting individual tracks in the developed plates. The plates available at the time the experiments were done were not sensitive enough to record the high energy portions of the tracks, and it was necessary to slow the protons down and then count the low energy ends. We used Ilford Nuclear Research plates,[7] type B.1. These plates show recognizable tracks for low energy protons (e.g., 20 Mev), but for protons of energies of the order of 100 Mev the number of developed grains per unit length of track is so small that the tracks get lost in the general background of developed grains. The method of slowing the protons down

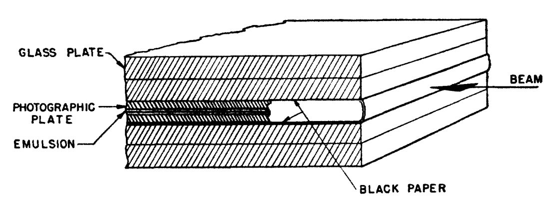

FIG. 3. Photographic plate "sandwich."

[5] M. M. Shapiro, Rev. Mod. Phys. **13**, 58 (1941).
[6] C. F. Powell and G. P. S. Occhialini, *Nuclear Physics in Photographs* (Clarendon Press, Oxford, 1947).
[7] Powell, Occhialini, Livesey, and Chilton, J. Sci. Inst. **23**, 102 (1946).

to a velocity such that they make recognizable tracks was to allow the proton beam to strike the edge of a "sandwich," as shown in Fig. 3. The sandwich is made up of two photographic plates placed emulsion to emulsion, with additional glass plates placed above and below. The photographic plates are wrapped in black paper, as shown in the figure. The dimension of the plates in the direction of the proton beam is greater than the range of the protons, so that the protons slow down and stop in the sandwich. It is assumed that protons scattered out of the emulsion are compensated for by others scattered in. This is only approximately true, since some protons make nuclear collisions in which they lose so much energy that they are effectively lost from the beam. The number of protons lost in this way would be expected to depend on the range, and hence on the energy of the protons.

Plates to be studied under the microscope were given an exposure in the cyclotron of about half a minute, and on these plates only a faint darkening was visible to the naked eye. In one of the early experiments, a set of plates was given a much heavier exposure in order to produce a more pronounced darkening. One of these plates is shown in Fig. 4. The dark streak on the plate is about one inch wide, corresponding to a one-inch slit through which the protons passed. The streak extends for about one and one-half inches from the edge of the plate and ends in a heavily darkened region at the position where the protons slow down and stop. At about a quarter of an inch from the edge of the plate there is an additional darkening, attributed to deuterons which were scattered from the dee but not broken up.

The slit system used with the photographic plate method is shown in Fig. 5. The first slits, and also the second slits, were one-half inch wide, and the two sets were about 12-inches apart. The photographic plates were arranged in sandwiches as previously described. The shielding and slit system was made of copper, shown by the shaded areas of Fig. 5. The plates were set at a height such that all of them received protons which left the target at an angle of $2\frac{1}{2}°$ down from the median plane. The photographic plates, with their shielding and slit system, were placed in the cyclotron in approximately the

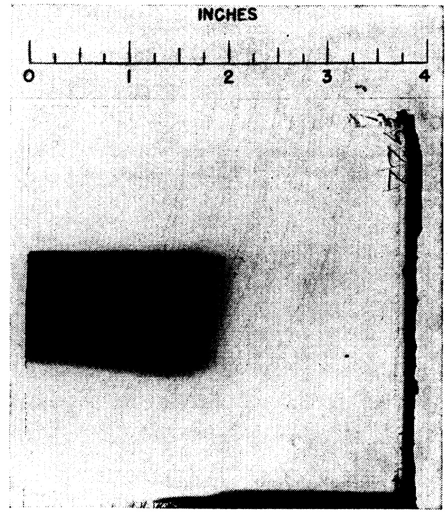

FIG. 4. Photographic plate showing darkening caused by protons and deuterons.

same position as that shown in Fig. 1 for the detectors in the carbon activation method.

The low energy ends of the tracks are recognized under the microscope by their close grain spacing, which makes the tracks appear nearly continuous. A portion of a field of view in the region of the low energy ends is shown in Fig. 6. The count was made by moving the field of view along the tracks (i.e., from left to right in Fig. 6) and adding up the number of low energy ends which stop in the emulsion. The numbers of tracks counted are shown in Table II. In addition to the statistical errors, there are also errors arising from the fact that the observer must use his judgment in deciding whether a track stops in the emulsion. It was assumed that the emulsion thickness was the same for all of the plates, and any variation in this thickness will introduce an error in the measurement. In the plates which we used, all of the tracks did not end at the position where the main group of tracks ended, but a few tracks were found at a much greater distance from the edge of the plate. Thus the observer had to use his judgment to decide how much of this "tail" to include in the count. The presence of this tail is explained by assuming that some of the proton trajectories lie partly in the black paper or in the open space caused by the folds in the black paper. The protons evidently pass through a short section of black

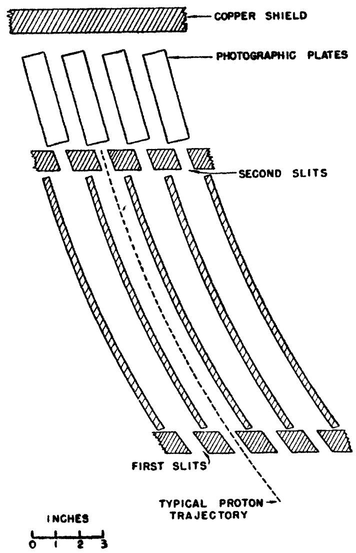

FIG. 5. Slit system used with photographic plate method.

paper or open space, and then through the glass part of the photographic plate, and then into the emulsion. (We realized after the experiments were done that we should put the paper on the outside of the entire package instead of just around the photographic plates.) Difficulties of this nature could, of course, be eliminated by placing in front of the sandwich a block of copper, or other material, of such thickness that most of the proton trajectory was in the block and only the last little bit in the sandwich. This refinement was not made in the runs from which the data of Table II were taken. The real difficulty with the photographic plate method as applied to this problem is that it takes so much effort to count a large number of tracks. There is plenty of plate area which could be used, and more tracks would undoubtedly be counted if there were no other method of getting the information. Since, however, the carbon activation method is able to get thousands of counts by automatic methods, it was not thought to be worth while to spend the time necessary to get really good results with photographic plate method.

The photographic plate data given in Table II have been plotted in Fig. 7. As in the case of the carbon activation data, the observed numbers of counts have been multiplied by the radius. Copper targets were used in both of the runs, the thickness being $\frac{1}{16}$ inch for run 1 and $\frac{1}{64}$ inch for run 2. In order that the data from the two runs could be compared with each other and with the carbon activation data, the values from run 2 have adjusted on the abscissa scale to the positions they would have had if a $\frac{1}{16}$-inch target had been used. In Fig. 7 the photographic plate data are compared with a calculated energy distribution which will be discussed in the next section. The irregularities in the plotted points are attributed to statistical errors, and other errors mentioned above.

At the time that the photographic plates were placed in the tank to study the protons coming from the target, additional plates were placed in positions to receive any negatively charged particles which might be coming from the target. Numerous straight, parallel tracks were found in these plates, but subsequent experimentation showed that they were not due to particles from the target at all but were due to neutral particles coming from the vicinity of the center of the cyclotron. The particles causing the tracks were later identified by L. W. Alvarez as deuterium atoms, presumably formed by a process in which a deuteron acquires an electron near the center of the cyclotron and moves outward as a neutral particle.

4. CALCULATED MOMENTUM DISTRIBUTIONS

The momentum distribution calculated from the transparent model of the stripping nucleus is given by Serber (reference 3, Eq. (9)) as follows:

$$P(\mathbf{p})d\mathbf{p}=(M\epsilon_d)^{\frac{1}{2}}/\pi^2(M\epsilon_d+p^2)^2d\mathbf{p}. \qquad (1)$$

In this equation, $P(\mathbf{p})$ is the probability that a proton will have a momentum $\mathbf{p}_0+\mathbf{p}$, where $\mathbf{p}_0$ is the momentum caused by the motion of the center of mass of the deuteron and $\mathbf{p}$ that caused by the motion within the deuteron. M is the mass of the proton, and ϵ_d is the binding energy of the deuteron. The small effect of the Coulomb deflection of the deuterons and protons in passing through the target has been neglected. The experimental results given in previous sections apply to the protons whose trajectories lie within the limited angular ranges admitted by the defining slits. The corresponding calculated distributions can be found from Eq. (1)

by integrating over the appropriate angular ranges. This integration will be done first for the carbon activation method, and then for the photographic plate method.

In the carbon activation method, the vertical angle, θ_v, at which the protons must leave the target in order to be detected varies from 6.9° for the detector nearest the target to 4.3° for the detector farthest away. For this range of angles the momentum distribution is not very sensitive to small changes in θ_v, and the average value of θ_v is a fairly good approximation. We introduce Cartesian coordinates with the z axis in the direction of the deuteron's motion, the x axis vertical, and the y axis horizontal. In this system the x-component of the momentum is given by

$$p_x \sim p_0\theta_v. \tag{2}$$

The slit system admits protons whose trajectories lie within a horizontal angle $\pm\theta_h$, where $\theta_h \sim 10°$, so that

$$|p_y| < p_h = p_0\theta_h. \tag{3}$$

The magnitude of the proton's momentum, p, is approximately equal to p_0+p_z. By writing $p_z = p - p_0$ in Eq. (1) and integrating over p_y between the limits $\pm p_h$, we find

TABLE II. Data from photographic plate method.

Radius (inches)	Number of counts run 1	run 2
33.2	—	81
34.1	228	107
35.1	218	250
36.0	240	249
36.8	322	238
37.8	339	270
38.8	252	421
39.6	189	497
40.5	90	211
41.4	46	167
42.3	41	163
43.2	37	78
44.1	—	76

$$\begin{aligned} P(p_x, p)dp_x dp \sim \{ & p_h[M\epsilon_d+p_x^2+(p-p_0)^2]^{-1} \\ & \times[M\epsilon_d+p_x^2+p_h^2+(p-p_0)^2]^{-1} \\ & +[M\epsilon_d+p_x^2+(p-p_0)^2]^{-\frac{3}{2}} \\ & \times\tan^{-1}p_h/[M\epsilon_d+p_x^2+(p-p_0)^2]^{\frac{1}{2}}\}dp_x dp. \end{aligned} \tag{4}$$

In this equation, and in other equations which follow, the constant factors have been omitted because we are interested only in the shape of the distribution.

The momentum distribution taken over all horizontal angles can be found from Eq. (4) by setting $p_x \to \infty$. This gives

$$P(p_x, p)dp_x dp \sim [M\epsilon_d+p_x^2+(p-p_0)^2]^{-\frac{3}{2}}dp_x dp. \tag{5}$$

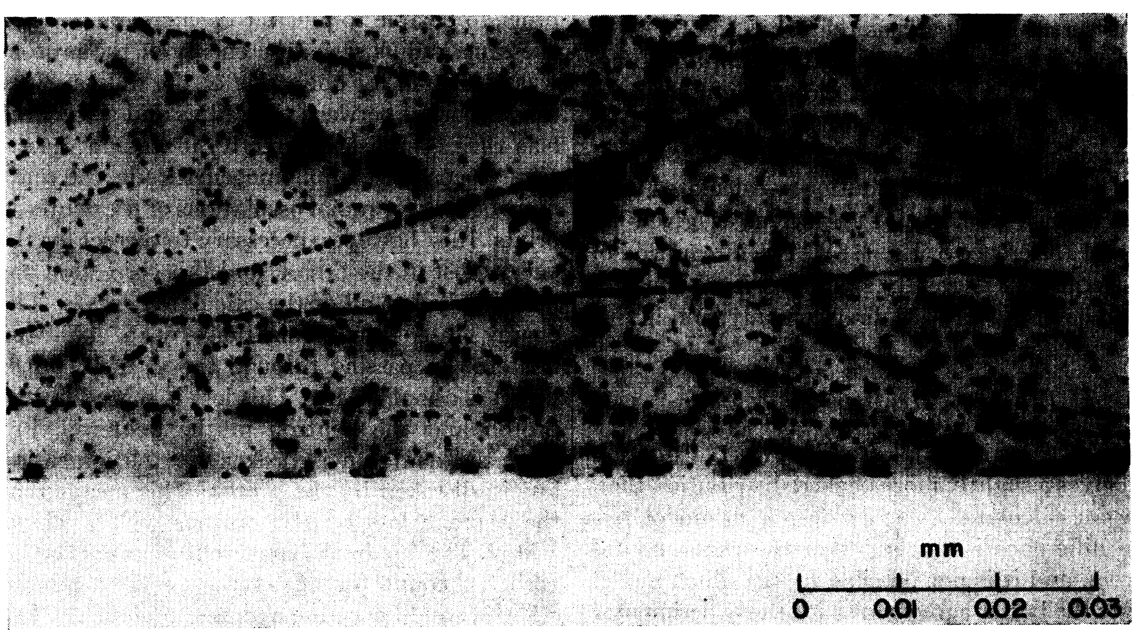

FIG. 6. Low energy ends of proton tracks (3-mm apochromatic objective lens). Beam direction is from the left.

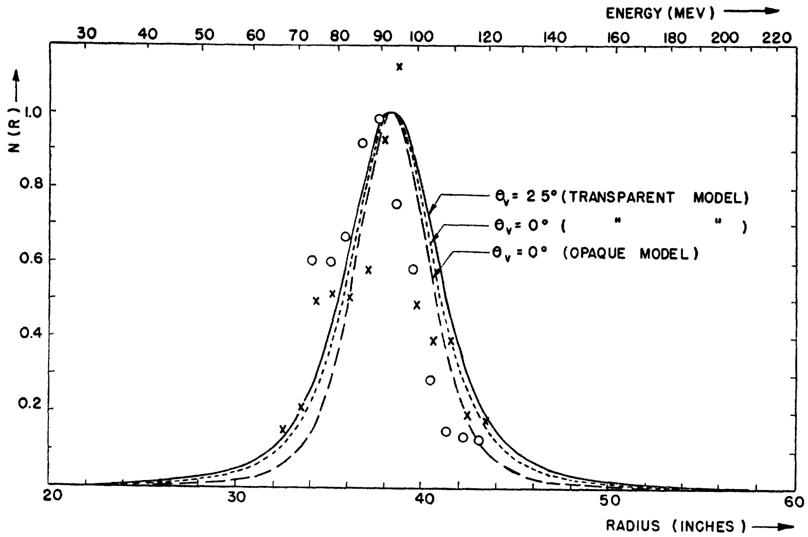

FIG. 7. Distribution measured with photographic plates. Ordinate gives numbers of protons in various momentum intervals. Circles, run 1; crosses, run 2. θ_v = vertical angle at which trajectory leaves the target. The curves are calculated distributions.

The momentum distributions given by Eqs. (4) (with $\theta_h=10°$) and (5) have been plotted in Fig. 2 for comparison with the experimental data from the carbon activation method.

In the photographic plate method, the defining slots cut out all the protons except those leaving the target at a very small horizontal angle. Thus, we can set p_y equal to zero in Eq. (1) and get

$$P(p_x, p)dp_xdp \sim [M\epsilon_d + p_x^2 + (p-p_0)^2]^{-2}dp_xdp. \quad (6)$$

The vertical angle θ_v has the value 2.5° for all of the photographic plates. The distribution function given by Eq. (6) is plotted in Fig. 7 for comparison with the photographic plate data. Curves are given for $\theta_v=2.5°$ and $\theta_v=0$.

The momentum distribution as calculated from the opaque model of the nucleus is given by Serber (reference 3, Eq. (18)). The integration of this equation is greatly simplified if we consider protons in the forward direction only, and in this case we get

$$P(p)dp \sim [M\epsilon_d + (p-p_0)^2]^{-5/2}dp. \quad (7)$$

This distribution is plotted in Fig. 7. Equation (7) gives a slightly more peaked distribution than the one calculated using a transparent model, but the difference is smaller than the experimental errors, and it is not possible to say which model gives the better agreement with the experimental data. The distribution function for the opaque model has not been worked out in detail for the carbon activation geometry, but here, too, the difference between the two models appears to be smaller than the experimental uncertainty.

The experimental data given in Figs. 2 and 7 have been plotted directly as a function of radius. The observed intensities were multiplied by the radius in order to take account of the vertical spread of the protons (i.e., to reduce the results to constant dp_z), and the resulting distributions were normalized but no corrections applied. In order to be able to plot the calculated curves on the same radius scale, the energy of the protons was measured for one value of the radius. Since a relationship between the radius and the energy was thus established directly, it was not necessary to correct for inhomogeneities in the magnetic field or for radial oscillations of the deuteron orbits. It is, however, necessary to correct for the energy lost in the target, and this correction has been applied to all of the calculated curves. The energy lost from ionization by a 190-Mev deuteron in passing through the $\frac{1}{16}$-inch copper target is about 7 Mev. This loss is shared by the proton and the neutron in the deuteron, but after the deuteron is broken up the ionization loss is all taken by the proton. This means that the average loss by the protons will be about 5 Mev. The Coulomb barrier effects discussed by Serber account for an average energy gain of 3.5 Mev, and hence the average total energy lost by the protons in passing through the target is about 1.5 Mev. This target loss has been taken account of by shifting all of the calculated curves toward the lower end of the radius scale by an amount equivalent to 1.5 Mev.

From Figs. 2 and 7 it is seen that the experimental distributions are in general agreement with those calculated from the stripping process described by Serber. The experimental data are not good enough to permit us to make a choice between the transparent model and the opaque model.

5. ACKNOWLEDGMENTS

The authors wish to express their appreciation to Professor Ernest O. Lawrence for his encouragement of this work. We are indebted to Professor Edwin M. McMillan, Professor Robert Serber, Professor R. L. Thornton, and Professor L. W. Alvarez for helpful discussions. We also wish to thank Mr. D. J. O'Connell for doing the microscope work associated with the photographic plate method, and Mr. Duane Sewell and the cyclotron crew for making bombardments.

This paper is based on work performed under Contract No. W-7405-eng-48, with the Atomic Energy Commission, in connection with the Radiation Laboratory, University of California, Berkeley, California.

PHYSICAL REVIEW VOLUME 73, NUMBER 7 APRIL 1, 1948

Temperature Dependence of Electron Energy Levels in Solids*

ALVIN RADKOWSKY
Catholic University, Washington, D. C.
(Received July 17, 1947)

In many crystalline insulators there is a temperature proportional displacement of the long wave-length absorption limit towards longer wave-lengths. These are crystals which have a broad, nearly structureless absorption which is caused by the transition of an electron from a full to an empty electron band. Previous attempts to explain this phenomenon have shown that the effects of thermal expansion are far too small to account for the observed shift. In this paper it is shown that there is a broadening of electron energy levels due to collisions with the thermally vibrating lattice which results in reducing the effective width of the "forbidden" energy region between occupied and conducting bands. Calculations indicate that, in polar crystals for which the observations have been made, this effect is of the proper magnitude to explain the experimental data. In non-polar crystals the effect would be very small. However, no absorption shift in non-polar crystals has been observed.

1. INTRODUCTION

(a) General Discussion of the Shift of Absorption with Temperature in Insulating Crystals

IT is well known that in many crystalline insulators there is a displacement of absorption toward longer wave-lengths with increasing temperature.[1,2] This is manifested in many cases by a deepening of the color. For example, ZnI, white at room temperature, becomes yellow at higher temperatures. This is due to the fact that the absorption, which at room temperature starts about 3600A and extends far into the ultraviolet, shifts into the blue at higher temperature.

The shift toward longer wave-lengths at higher temperature applies to excitation lines as well as to the long wave absorption limit of the main absorption. However, this paper treats the latter case primarily, although, as indicated at the end

* Adapted from a dissertation submitted to the faculty of the Graduate School of Arts and Sciences of the Catholic University of America in partial fulfillment of the requirements for the degree of Doctor of Philosophy.

[1] F. Möglich and R. Rompe, Zeits. f. Physik **119**, 472 (1942), containing data of the shift of the absorption limit. H. Fesefeldt, *ibid.* **64**, 623 (1930) the data of which probably pertains to shift of excitation lines (see Section III).

[2] There is also a much larger shift which sets in suddenly at higher temperature. Möglich and Rompe state that this is due to "multiple collisions." Naturwiss. **29**, 105, Feb. 21, and 120, Feb. 28 (1941).

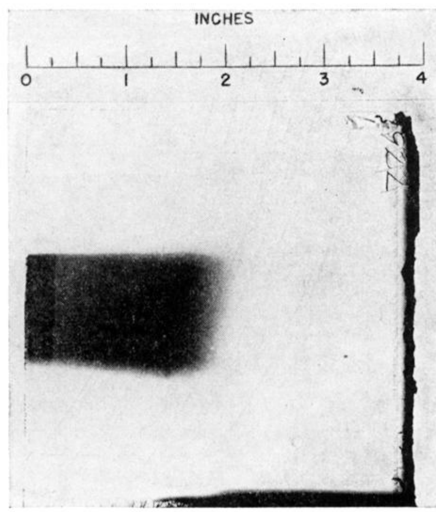

FIG. 4. Photographic plate showing darkening caused by protons and deuterons.

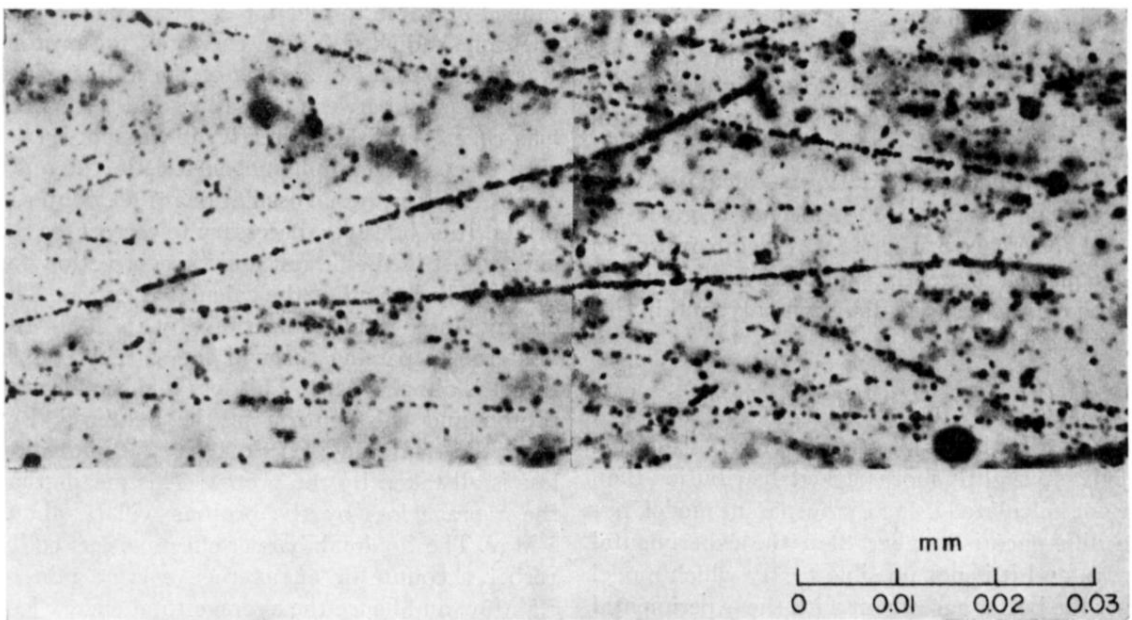

FIG. 6. Low energy ends of proton tracks (3-mm apochromatic objective lens). Beam direction is from the left.